

# Human sterol 14 $\alpha$ -demethylase as a target for anticancer chemotherapy: towards structure-aided drug design<sup>1</sup>

Tatiana Y. Hargrove,\* Laura Friggeri,\* Zdzislaw Wawrzak,<sup>†</sup> Suneethi Sivakumaran,\* Eugenia M. Yazlovitskaya,<sup>§</sup> Scott W. Hiebert,\* F. Peter Guengerich,\* Michael R. Waterman,\* and Galina I. Lepesheva<sup>2,\*</sup>

Department of Biochemistry,\* Vanderbilt University School of Medicine, Nashville, TN 37232; Synchrotron Research Center,<sup>†</sup> Life Science Collaborative Access Team, Northwestern University, Argonne, IL, 60439; and Department of Medicine,<sup>§</sup> Vanderbilt University Medical Center, Nashville, TN 37232

**Abstract** Rapidly multiplying cancer cells synthesize greater amounts of cholesterol to build their membranes. Cholesterol-lowering drugs (statins) are currently in clinical trials for anticancer chemotherapy. However, given at higher doses, statins cause serious side effects by inhibiting the formation of other biologically important molecules derived from mevalonate. Sterol 14 $\alpha$ -demethylase (CYP51), which acts 10 steps downstream, is potentially a more specific drug target because this portion of the pathway is fully committed to cholesterol production. However, screening a variety of commercial and experimental inhibitors of microbial CYP51 orthologs revealed that most of them (including all clinical antifungals) weakly inhibit human CYP51 activity, even if they display high apparent spectral binding affinity. Only one relatively potent compound, (*R*)-*N*-(1-(3,4'-difluorobiphenyl-4-yl)-2-(1*H*-imidazol-1-yl)ethyl)-4-(5-phenyl-1,3,4-oxadiazol-2-yl)benzamide (VFV), was identified. VFV has been further tested in cellular experiments and found to decrease proliferation of different cancer cell types. The crystal structures of human CYP51-VFV complexes (2.0 and 2.5 Å) both display a 2:1 inhibitor/enzyme stoichiometry, provide molecular insights regarding a broader substrate profile, faster catalysis, and weaker susceptibility of human CYP51 to inhibition, and outline directions for the development of more potent inhibitors.—Hargrove, T. Y., L. Friggeri, Z. Wawrzak, S. Sivakumaran, E. M. Yazlovitskaya, S. W. Hiebert, F. P. Guengerich, M. R. Waterman, and G. I. Lepesheva. Human sterol 14 $\alpha$ -demethylase as a target for anticancer chemotherapy: towards structure-aided drug design. *J. Lipid Res.* 2016. 57: 1552–1563.

**Supplementary key words** cancer • cholesterol • cholesterol/biosynthesis • enzymology/enzyme mechanisms • membranes • X-ray crystallography • drug therapy/hypolipidemic drugs; cytochrome P450 • inhibition

Sterol biosynthesis is an essential metabolic pathway in most eukaryotes and in some bacteria (1). Sterols (cholesterol in humans, sitosterol in plants, ergosterol and its C24-alkylated derivatives in fungi and protozoa) are required

This work was supported by National Institute of General Medical Sciences Grant GM067871 (to G.I.L.). The content is solely the responsibility of the authors and does not necessarily represent the official views of the National Institutes of Health.

Manuscript received 12 May 2016 and in revised form 15 June 2016.

Published, JLR Papers in Press, June 16, 2016

DOI 10.1194/jlr.M069229

components of eukaryotic membranes, where they control fluidity and permeability and modulate functions of membrane-bound enzymes, receptors, and ion channels. These sterols also serve as precursors for multiple regulatory molecules that are crucial for cell division, growth, and development (2–4).

Sterol biosynthesis is the target for many drugs. Statins, as inhibitors of HMG-CoA reductase (EC.1.1.1.34), act upstream in the pathway at the step of mevalonate production and serve as major cholesterol-lowering drugs in humans (5, 6), while azoles, as inhibitors of fungal and protozoan cytochrome P450 sterol 14 $\alpha$ -demethylase (CYP51, EC.1.14.13.70), act downstream in the pathway at its postsqualene portion and are widely used as antimicrobial agents (1, 7, 8).

Human CYP51 [ $<35\%$  amino acid sequence identity with fungal and  $<25\%$  identity with protozoan orthologs (9)] has also been considered as a drug target. Several attempts to develop CYP51 inhibitors as cholesterol-lowering agents have been undertaken (10–13), yet they were eventually dropped because of the phenomenal success of statins, which are currently the most frequently prescribed medications (5, 6). Statins have been reported to be effective not only as anti-cardiovascular agents, but also for other cholesterol-related diseases [e.g., Alzheimer's (14) and Parkinson's diseases (15), multiple sclerosis (16)] and are currently in clinical trials for different types of cancer (17–25), which is quite rational because cancer cells can be viewed as unicellular eukaryotic parasites, multiplying uncontrollably within the human body. For multiplication, they need cholesterol. The

Abbreviations: BrdU, 5-bromodeoxyuridine; CYP51, cytochrome P450 sterol 14 $\alpha$ -demethylase; HPCD, hydroxypropyl- $\beta$ -cyclodextrin; NTA, Ni<sup>2+</sup>-nitrilotriacetate; PDB, Protein Data Bank; rms, root-mean-square; (*S*)-VFV, *S*-enantiomer of (*R*)-*N*-(1-(3,4'-difluorobiphenyl-4-yl)-2-(1*H*-imidazol-1-yl)ethyl)-4-(5-phenyl-1,3,4-oxadiazol-2-yl)benzamide; VFV, (*R*)-*N*-(1-(3,4'-difluorobiphenyl-4-yl)-2-(1*H*-imidazol-1-yl)ethyl)-4-(5-phenyl-1,3,4-oxadiazol-2-yl)benzamide.

<sup>1</sup>The coordinates and structure factors for human sterol 14 $\alpha$ -demethylase (CYP51) in complex with VFV in space groups C121 and P1 have been deposited in the Protein Data Bank (PDB) with accession numbers 4UHI and 4UHL, respectively.

<sup>2</sup>To whom correspondence should be addressed.

e-mail: galina.i.lepesheva@vanderbilt.edu

exact anticancer mechanism of statins remains unclear, yet recent data show that they affect the adhesion, invasion, and migration processes and induce apoptosis of cancer cells by disrupting integrity of lipid rafts in their membrane (26–32). However, by blocking an early step in the pathway, statins affect not only production of cholesterol but also the formation of other physiologically important compounds [e.g., ubiquinone, dolichols, prenylated proteins (33)], and therefore, in long-term use, can cause dose-dependent side effects [mainly myopathy (34–37)] leading to discontinuation of treatment in up to 20% of patients (38, 39). Also, because, due to uptake transporters, statins generally target the liver (where ~70% of cholesterol is synthesized), in clinical trials for cancer they have to be used at much higher doses (33) to reach other organs and tissues. Accordingly, although sometimes supplemented with intermediates [e.g., ubiquinone (17)], they produce stronger side effects. Due to the side effects of statins, alternative drugs that target cholesterol biosynthesis in humans more specifically would be highly desirable, and CYP51, the lanosterol demethylase, is a target of interest in that several more distal (post-lanosterol) steps in the cholesterol synthesis pathway are known to be associated with hereditary diseases when they are attenuated (40). For instance, a loss of the sterol 7-reductase (DHCR7) is associated with a severe disease, Smith-Lemli-Opitz syndrome (41). Deficiency in the 3 $\beta$ -hydroxysteroid dehydrogenase (NSDHL) is responsible for congenital hemidysplasia, ichthyosiform nevus, and limb defects (CHILD) syndrome (42). Mutations in the  $\Delta^7, \Delta^8$ -sterol isomerase (EBP) are associated with Conradi-Hünemann-Happle syndrome, or X-linked dominant chondrodysplasia punctata type 2 (CDPX2) (40), and mutations in sterol 5-desaturase (SC5D) cause lathosterolosis (43). Compared with these problems, attenuating lanosterol 14-demethylation seems very favorable.

It is now generally accepted that cancer cells have elevated levels of cholesterol in lipid rafts and contain more lipid rafts than their normal cell line counterparts (26, 27, 29, 31, 44). Enhanced expression of enzymes of the cholesterol pathway has been reported in many cancer cell types (31, 45–47). Furthermore, certain types of cancer exhibit CYP51 gene amplification (<http://www.cbioportal.org>). It is likely that the earlier attempts to develop human CYP51 inhibitors were unsuccessful because they concentrated on substrate analogs, which had rather low inhibitory potency (10) and could not compete in efficiency with statins. Here, we performed a biochemical characterization of human CYP51, including substrate preferences, catalytic parameters, inhibition, and the structure of a complex with (*R*)-*N*-(1-(3,4'-difluorobiphenyl-4-yl)-2-(1*H*-imidazol-1-yl)ethyl)-4-(5-phenyl-1,3,4-oxadiazol-2-1) benzamide (VFV), the most potent inhibitor that we have identified. VFV was further tested in cancer cells and found to be active against different types of cancers.

## MATERIALS AND METHODS

### Materials

VNI, VNT, VNF, and VFV were synthesized by the Chemical Synthesis Core Facility (Vanderbilt Institute of Chemical Biology) (48).

VFV-Cl was synthesized using the same procedure. Voriconazole, ketoconazole, itraconazole, and posaconazole were purchased from Santa Cruz Biotechnology (Santa Cruz, CA); fluconazole was from ICN Biomedicals. Hydroxypropyl- $\beta$ -cyclodextrin (HPCD) was purchased from Cyclodextrin Technology Development (Gainesville, FL). DEAE- and CM-Sepharose were from GE Healthcare, and Ni<sup>2+</sup>-nitrilotriacetate (NTA) agarose was purchased from Qiagen. All cell lines were purchased from American Type Culture Collection (Manassas, VA).

### Protein expression, purification, and crystallization

*Trypanosoma cruzi*, *Aspergillus fumigatus*, and full-length human CYP51 and *T. brucei* and rat NADPH-cytochrome P450 reductase were expressed in *Escherichia coli* and purified as described previously (49, 50). The full-length proteins were used for functional studies (ligand binding, enzymatic activity, and inhibition). For crystallization, human CYP51 [UniProt protein accession number Q16850, 503 amino acid residues plus the (His)<sub>6</sub>-tag at the C terminus, 57,300 Da] was truncated (458 amino acid residues, 53,400 Da) as described previously (51). Briefly, the 50-amino acid membrane anchor sequence at the N terminus (up to the conserved CYP51 proline, Pro61 in human CYP51) was replaced with the MAKKTSSKGKL-fragment (52) and subcloned into the pCW expression vector using the *Nde*I (5') and *Hind*III (3') sites. The truncated human CYP51 was purified in two steps, including affinity chromatography on Ni<sup>2+</sup>-NTA agarose and cation exchange chromatography on CM-Sepharose. The Ni<sup>2+</sup>-NTA bound protein was washed with 10 bed volumes of 50 mM potassium phosphate buffer (pH 7.2) containing 100 mM NaCl, 10% glycerol (v/v), 1 mM imidazole, and 0.1% Triton X-100 (v/v) and then with 20 mM potassium phosphate buffer (pH 7.2) containing 500 mM NaCl, 10% glycerol (v/v), and 5 mM imidazole until the Triton X-100 was eliminated (as judged by *A*<sub>280</sub> measurements). The P450 was eluted with a linear gradient of imidazole (10–80 mM), and the fractions with a spectrophotometric index (*A*<sub>425</sub>/*A*<sub>280</sub>)  $\geq 1$  were pooled and concentrated using an Amicon Ultra 50 K (Millipore) concentration device to a volume of 1–2 ml. The concentrated protein was then diluted 10-fold with 20 mM potassium phosphate buffer (pH 7.2) containing 10% glycerol (v/v) and 0.1 mM EDTA (CM-buffer) and applied to a CM-Sepharose column (5 ml bed volume) equilibrated with CM-buffer containing 50 mM NaCl. The column was washed with five bed volumes of equilibration buffer and then 40 bed volumes of CM-buffer with an increasing linear gradient of NaCl (50–200 mM). The protein was eluted with CM-buffer containing 300 mM NaCl, the fractions containing the enzyme were pooled, and VFV was added from a 10 mM DMSO stock solution (molar ratio VFV/CYP51 = 2.5:1). Then the complex (complex 1) was concentrated to about 500  $\mu$ M P450 using an Amicon Ultra 50 K concentration device, aliquoted, frozen in liquid nitrogen, and stored at  $-80^{\circ}\text{C}$  until use. The yield was between 300 and 400 nmol/liter culture. The purity was verified by SDS-PAGE. Alternatively, when human CYP51 was copurified with the inhibitor (complex 2), all of the buffer solutions used for CM-chromatography contained 10  $\mu$ M VFV. The sample was concentrated to about 500  $\mu$ M P450 and used for crystallization immediately. The crystals were obtained by the hanging drop vapor diffusion technique. Crystals of complex 1 were grown at 20°C. Equal volumes of the P450-VFV complex solution preincubated with 0.18 mM Thesit (Hampton Research) and 5.5 mM tris(carboxyethyl)phosphine were mixed with mother liquor [0.2 M trisodium citrate dehydrate, 0.10 mM HEPES (pH 7.5), and 12% PEG 8,000 (w/v)] and equilibrated against the reservoir solution. Crystals of complex 2 were grown at 18°C by mixing equal volumes of the complex solution preincubated with 5.8 mM CYMAL-5 (Anagrade) and 5.5 mM tris(carboxyethyl)phosphine

with 0.20 M potassium fluoride (pH 7.2) and 15% PEG 6,000 (w/v). In both cases crystals appeared after several days and were cryoprotected by soaking them in mother liquor with 30% glycerol (v/v) and flash-cooled in liquid nitrogen.

### Spectroscopic measurements and ligand binding assays

UV-visible absorption spectra were recorded using a dual-beam Shimadzu UV-2401PC spectrophotometer. P450 concentrations were determined from the Soret band intensity using  $\epsilon_{417}$  117  $\text{mM}^{-1} \text{cm}^{-1}$  for the low-spin ferric form of the protein or  $\Delta\epsilon_{450-490}$  91  $\text{mM}^{-1} \text{cm}^{-1}$  for the reduced carbon monoxide difference spectra; the spin state of the P450 samples was estimated from the absolute absorbance spectra (53). Substrate binding was monitored as a "type I" spectral response (blue shift in the Soret band maximum from 417 to 393 nm) (54) reflecting low-to-high spin transition of the ferric P450 heme iron as a result of displacement of the heme-coordinated water molecule (50). Various aliquots of sterols (dissolved in 45% HPCD, w/v) (49) were added to the sample cuvette (1 cm optical path length), and the same volume of HPCD was added to the reference cuvette. The apparent dissociation constants of the enzyme-substrate complex ( $K_d$ ) were calculated in Prism 6 software (GraphPad, La Jolla, CA) by fitting the data for the substrate-induced absorbance changes in the difference spectra  $\Delta(A_{390}-A_{420})$  versus substrate concentration to a one site-total binding equation (binding-saturation). Inhibitor binding was monitored as a "type II" spectral response (red shift in the Soret band maximum from 417 to 421–427 nm) (54) reflecting coordination of the basic heterocyclic nitrogen to the P450 heme iron (55). Difference spectra were generated by recording the P450 absorbance in a sample cuvette (5 cm optical path length) versus the absorbance in a reference cuvette, both containing the same amount of the protein. Aliquots of azoles (dissolved in

DMSO) were added to the sample cuvette in the concentration range of 0.1–20  $\mu\text{M}$  (5–200  $\mu\text{M}$  for fluconazole). At each step, the corresponding volume of DMSO was added to the reference cuvette. The apparent dissociation constants of the enzyme-ligand complex ( $K_d$ ) were calculated in GraphPad Prism 6 software by fitting the data for the ligand-induced absorbance changes in the difference spectra  $\Delta(A_{\text{max}}-A_{\text{min}})$  versus ligand concentration to the quadratic equation 1 (for tight-binding ligands),

$$\Delta A = (\Delta A_{\text{max}}/2E) \left[ (L+E+K_d) - \left( (L+E+K_d)^2 - 4LE \right)^{0.5} \right] \quad (\text{Eq. 1})$$

where (L) and (E) are the total concentrations of ligand and enzyme used for the titration, respectively.

### Reconstitution of catalytic activity, kinetic analysis, and CYP51 inhibition assays

The standard reaction mixture (49) contained 0.5  $\mu\text{M}$  P450 and 1.0  $\mu\text{M}$  cytochrome P450 reductase (*T. brucei* or rat for *T. cruzi* or human and *A. fumigatus* CYP51 orthologs, respectively), 100  $\mu\text{M}$  L- $\alpha$ -1,2-dilauroyl-*sn*-glycerophosphocholine, 0.4 mg/ml isocitrate dehydrogenase, and 25 mM sodium isocitrate in 50 mM potassium phosphate buffer (pH 7.2) containing 10% glycerol (v/v). After addition of the radiolabeled ( $[3\text{-}^3\text{H}]$ ) sterol substrates ( $\sim 4,000$  dpm/nmol; dissolved in 45% HPCD, w/v) (56), the mixture was preincubated for 30 s at 37°C in a shaking water bath, and the reaction was initiated by the addition of 100  $\mu\text{M}$  NADPH and stopped by extraction of the sterols with 5 ml of ethyl acetate. The extracted sterols were dried, dissolved in  $\text{CH}_3\text{OH}$ , and analyzed by a reversed-phase HPLC system (Waters) equipped with a  $\beta$ -RAM detector (INUS Systems) using a NovaPak octadecylsilane ( $\text{C}_{18}$ ) column (particle size 4

TABLE 1. Data collection and refinement statistics for human CYP51 complexes with VFV crystallized in  $\text{C}_121$  and P1 space groups

PDB Code	4UHI	4UHL
Data collection		
Wavelength (Å)	0.97872	0.97872
Space group	C121	P1
Cell dimensions		
a, b, c (Å)	168.663, 145.869, 115.987	111.210, 111.500, 118.480
$\alpha, \beta, \gamma$ (°)	90.00, 127.15, 90.00	64.09, 75.07, 62.42
Number of molecules in asymmetric unit	4	8
Solvent content (%)	52.4	53.7
Resolution (last shell) (Å)	98.85–2.04 (2.28–2.04)	54.3–2.5 (2.56–2.50)
$R_{\text{merge}}$ (last shell)	0.069 (0.486)	0.055 (0.622)
$I/\sigma$ (last shell)	13.2 (3.0)	14.0 (2.0)
Completeness (last shell) (%)	98.8 (98.6)	98.5 (97.7)
Redundancy (last shell)	4.6 (4.7)	3.9 (4.0)
Refinement		
Resolution (Å)	50.0–2.04	54.3–2.50
R-factor	0.215	0.192
R-free	0.233	0.237
Reflections used	133,884	146,548
Test set size (%)	5.3	5.3
Rms deviations from ideal geometry		
Bond lengths (Å)	0.009	0.005
Bond angles (°)	0.98	0.87
Ramachandran plot		
Residues in favorable regions (%)	97.5	96.7
Residues in allowed regions (%)	99.9	99.9
Outliers (%)	0.06	0.08
Model		
Number of atoms (mean B-factor, Å <sup>2</sup> )	15,422 (40.5)	30,632 (64.4)
Number of residues per molecule	A/B/C/D	A–H
Protein	442/442/442/442 (40.5 $\pm$ 3.3)	445 (64.8 $\pm$ 3.5)
Heme	1/1/1/1 (28.6 $\pm$ 3.0)	1 (52.4 $\pm$ 3.1)
Ligand (VFV)	2/2/2/2 (36.8 $\pm$ 2.0; 44.3 $\pm$ 3.3 SE)	2 (45.4 $\pm$ 2.6; 56.7 $\pm$ 2.8)
Water	654 (41.7)	928 (60.9)

$\mu\text{m}$ ,  $3.9 \times 150 \text{ mm}$ ) and a linear gradient water/ $\text{CH}_3\text{CN}:\text{CH}_3\text{OH}$  (1.0:4.5:4.5, v/v/v) (solvent A) to  $\text{CH}_3\text{OH}$  (solvent B), increasing from 0 to 100% B for 30 min at a flow rate of 1.0 ml/min. For steady-state kinetic analysis, the reactions were run for 60 s at  $37^\circ\text{C}$ , and the sterol concentration range was 6–50  $\mu\text{M}$ . Michaelis-Menten parameters were calculated using GraphPad Prism 6, with the reaction rates (nanomoles of product formed per nanomole of P450 per minute) being plotted against total substrate concentration. The inhibitory potencies of azoles on *T. cruzi*, *A. fumigatus*, and human CYP51 activity were compared on the basis of decreases in substrate conversion in 60 min reactions (50, 51, 57, 58).

## Cancer cell proliferation assays

**Acute myeloid leukemia.** Kasumi-1 cells were split to a concentration of  $2.5 \times 10^5$  cells/ml in RPMI medium containing 10% Fetal-Plex (v/v), 1% penicillin-streptomycin (w/v), and 1% glutamine (w/v) and treated with 50  $\mu\text{M}$  VFV, 50  $\mu\text{M}$  Senantiomer of VFV [(*S*)-VFV] (from 5 mM stock solutions in DMSO), or the vehicle (1% DMSO). Aliquots (100  $\mu\text{l}$ ) of treated cells were plated in 96-well tissue culture plates every day for 7 days and 10  $\mu\text{l}$  of Alamar blue (Biosource, USA) were added. Cell proliferation was monitored by measuring fluorescence emission at 590 nm, as described previously (57).

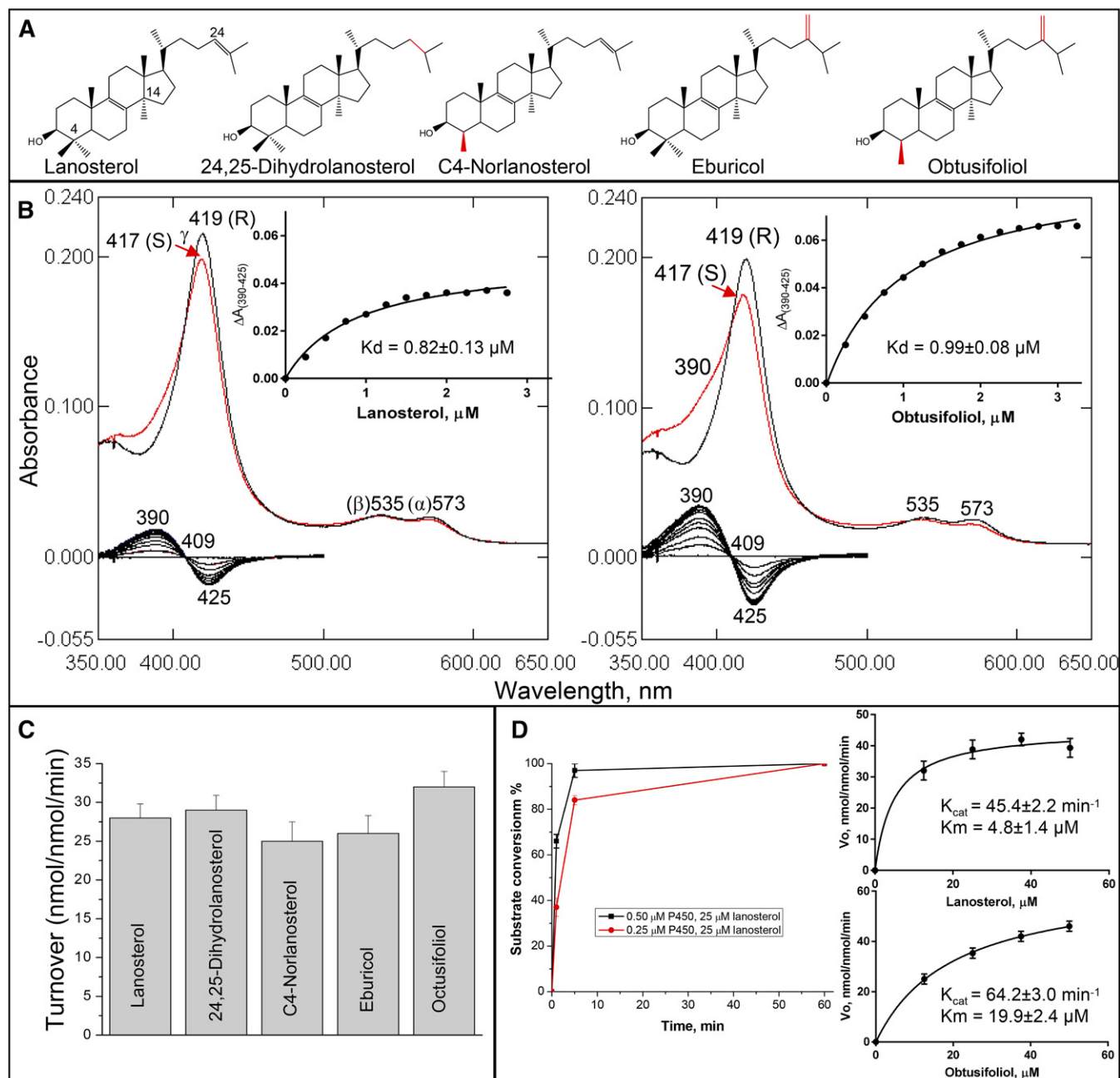


**Fig. 1.** Substrate binding and catalysis by human CYP51. A: CYP51 substrates: structural differences (relatively to lanosterol) are marked in red. B: Spectral response of human CYP51 to lanosterol and obtusifoliol. P450 concentration  $\sim 1.7 \mu\text{M}$ , optical pathlength 1 cm. Absorbate (top) and difference (bottom) absorbance spectra. The low-to-high spin transitions (saturation with lanosterol and obtusifoliol) were 18 and 36%, respectively. Titration curves are presented in the insets; the corresponding calculated binding parameters are given in Table 2. C: Experimental catalytic turnovers of human CYP51 at 0.5  $\mu\text{M}$  P450 and 50  $\mu\text{M}$  sterol substrate, 1 min reaction. D: Time course with 0.5 and 0.25  $\mu\text{M}$  P450 and Michaelis-Menten plots at 0.25  $\mu\text{M}$  P450 (1 min reaction); see also Table 3.

TABLE 2. Substrate binding parameters calculated from the spectral response of human CYP51 to the binding of lanosterol and obtusifoliol

Substrate	$\Delta A_{\max}$		$K_d$ ( $\mu\text{M}$ )	$\Delta A_{\max}/K_d^a$
	Absorbance Units/ $\mu\text{M}$ P450/cm	Low-to-High Spin Transition (%)		
Lanosterol	$0.029 \pm 0.01$	26	$0.82 \pm 0.13$	32
Obtusifoliol	$0.056 \pm 0.01$	51	$0.99 \pm 0.08$	52

<sup>a</sup>Apparent binding efficiency.

Lung cancer, hormone-responsive and -nonresponsive breast cancer, and skin cancer cells. A549, MCF-7, MB-MDA-436, and A-431 cancer cells were plated in 96-well tissue culture plates ( $10^5$  cells/ml in 100  $\mu\text{l}$  per well of DMEM supplemented with 10% FBS, v/v). After 6 h, VFV (5–25  $\mu\text{M}$ , from 100 $\times$  stock solutions in 25% DMSO/34% HPCD, v/v) or the vehicle (0.25% DMSO/0.34% HPCD) was added. Cell proliferation was assessed after 24 h of incubation by measuring incorporation of 5-bromodeoxyuridine (BrdU) using a BrdU cell proliferation ELISA (colorimetric) kit (Exalpha Biologicals) according to the manufacturer's instructions. BrdU incorporation was quantified by absorbance at 450 nm.

The experiments were performed three times, each in triplicate; the *P* value was calculated using Student's *t*-test;  $P \leq 0.05$  was considered statistically significant.

#### Data collection, X-ray structure solution, model building, and refinement

All data were collected at 100 K using synchrotron radiation at beamline 21-ID-F (LS-CAT, Argonne, IL), MAR225 CCD detector. Processing and scaling were accomplished with Mosflm and Aimless software [CCP4 Program Suite 6.5.019 (59)]. Data collection and refinement statistics are summarized in **Table 1**. The structures were solved by molecular replacement in PhaserMR (CCP4 Suite). The search models were 3LD6 for complex 1 and 4UHI for complex 2. The structures were then subjected to iterative cycles of model building and refinement with Coot and Refmac5 (CCP4 Suite). Structure superpositions were done in LSQkab (CCP4 Suite), and structural figures were prepared with Pymol, Chimera, and Accelrys. The coordinates and structure factors are deposited in the Protein Data Bank (PDB) under PDB codes 4UHI and 4UHL.

## RESULTS AND DISCUSSION

CYP51s are key enzymes in sterol biosynthesis and are found in all biological kingdoms, catalyzing three consecutive monooxygenation reaction cycles to remove the 14 $\alpha$ -methyl group from the cyclized sterol precursors (**Fig. 1A**) (9). Microbial CYP51 enzymes are currently the leading targets in antifungal chemotherapy (7) and emerging targets in kinetoplastid protozoa (8). The objective of this work was to examine structure/function relationships and drugability of human CYP51.

TABLE 3. Steady-state kinetic parameters for 14 $\alpha$ -demethylation of lanosterol and obtusifoliol by human CYP51

Substrate	Maximal Turnover Rate <sup>a</sup> (nmol/nmol/min)	Michaelis-Menten Parameters		
		$k_{\text{cat}}$ ( $\text{min}^{-1}$ )	$K_m$ ( $\mu\text{M}$ )	$k_{\text{cat}}/K_m$ ( $\text{min}^{-1} \mu\text{M}^{-1}$ )
Lanosterol	$42 \pm 1$	$45 \pm 2$	$4.8 \pm 1.4$	9.5
Obtusifoliol	$46 \pm 1$	$64 \pm 3$	$20 \pm 2$	3.2

<sup>a</sup>Experimentally observed.

#### Substrate binding profile and catalytic parameters

Unlike CYP51 orthologs from other biological kingdoms, which usually express high preferences toward their physiological substrates [e.g., obtusifoliol in plants, algae, *Leishmania*, and *Trypanosoma brucei* (49, 53); eburicol in *Aspergillus fumigatus* and *Trypanosoma cruzi* (50, 60)], the human enzyme binds all of the five natural CYP51 substrates (**Fig. 1A**) and catalyzes their 14 $\alpha$ -demethylation quite efficiently (**Fig. 1C**). The observed maximal amplitudes of the spectral response to addition of substrate (blue shift in the Soret band maxima), however, did not exceed 40% of the maximum low-to-high spin state transition in the P450 heme iron. The examples of spectral titration of human CYP51 with its physiological substrate, lanosterol, and with obtusifoliol are presented in **Fig. 1B**. Although the apparent  $K_d$  values are comparable (0.82 and 0.99  $\mu\text{M}$  for lanosterol and obtusifoliol, respectively), the apparent binding efficiency of obtusifoliol is higher ( $\sim 1.6$ -fold) than the efficiency of binding of lanosterol, due to the larger amplitude of the spectral change. This larger amplitude of the spectral response may be connected with the relatively better aqueous solubility of obtusifoliol (logP 8.0 vs. 8.2 for lanosterol), although it cannot be excluded that the positioning of the (bulkier) methylene group at the C24 atom of obtusifoliol within the enzyme active site somehow requires a higher degree of water displacement from the coordinating sphere of the P450 heme iron [i.e., binding of eburicol (logP 8.6) produces even a little larger spectral amplitude (unpublished observations)]. Steady-state kinetic analysis also indicates faster oxidation of obtusifoliol by human CYP51, although the catalytic efficiency with lanosterol was  $\sim 3$ -fold higher due to the 4-fold lower  $K_m$  value (**Fig. 1D**, **Table 3**). The observed catalytic turnover numbers were 42 and 46  $\text{min}^{-1}$  for lanosterol and obtusifoliol, respectively.

Thus, in comparison with the orthologs from other phyla, human CYP51 appears to be the least substrate selective (allowing all naturally occurring variations in the composition of the C4 and C24 atom substituents in the sterol molecule, see **Fig. 1A**) and has the highest CYP51 rate reported to date.

#### Inhibition with clinical antifungal azoles and experimental antiprotozoan drug candidates

In our search for new inhibitors of CYP51s from human pathogens, we concomitantly conducted the control experiments evaluating the inhibitory effects of these compounds on the activity of human CYP51, e.g. (51, 55, 57, 60, 61). A broad variety of structurally different molecular chemotypes

was screened, but only one relatively potent inhibitor has been identified. **Figure 2A** compares systemic clinical antifungal drugs and some of our experimental compounds that are under development as antiprotozoan agents (48, 62) as inhibitors of protozoan (*T. cruzi*), fungal (*A. fumigatus*), and human CYP51 enzymes. In these experiments, we used a 60 min reaction because the longer incubation time affords higher sensitivity and, therefore, is helpful in screening out less effective inhibitors (48, 51, 57). Interestingly, under the same experimental conditions, while only a 2-fold molar excess over the enzyme was needed for the most potent compounds to cause complete inhibition of *T. cruzi* CYP51 (VNI derivatives) or 80–95% inhibition of *A. fumigatus* CYP51 (voriconazole, posaconazole, and VNI), human CYP51 displayed resistance to inhibition even at a 50-fold molar excess of the compounds. VFV was the only compound that acted as a fairly strong human CYP51 inhibitor, preventing 14 $\alpha$ -demethylation of >60% of lanosterol under these conditions. For comparison, when the effects of VFV and its S-enantiomer (*S*)-VFV (see Fig. 2A) on the initial rate of human CYP51 reaction were monitored, both compounds were able to attenuate substrate conversion (Fig. 2B), with the IC<sub>50</sub> values being 0.5 and 50  $\mu$ M, respectively. This effect was originally observed for protozoan CYP51 (57) and can be explained by the ability of the substrate to compete with heme-coordinating inhibitors in the CYP51 active site. With human CYP51, most compounds that did not show any inhibition in a 60 min reaction still displayed relatively strong binding affinities to the enzyme upon spectral titration (apparent  $K_d$  values are shown in Fig. 2A).

Overall, the observation that the activity of human CYP51 is weakly affected by the heme-binding ligands suggests that human CYP51 has specific features that define its intrinsically weaker susceptibility to inhibition, VFV being the only known relatively strong inhibitor of this enzyme.

### Inhibitory effects of VFV on proliferation of different types of cancer cells

Our experimental CYP51 structure-based VNI derivative, VFV, was designed to extend the antiprotozoal spectrum of activity (48, 62). VFV has low cytotoxicity [e.g., NIH/3T3 mouse embryonic fibroblasts, EC<sub>25</sub> >50  $\mu$ M (41)], excellent cellular permeability, favorable pharmacokinetics, broad tissue distribution, weak inhibitory effects on human drug-metabolizing P450s, and no adverse side effects when used in vivo in mouse models of Chagas disease and visceral leishmaniasis (62). Although the potency of VFV for inhibiting human CYP51 is less than for microbial orthologs (Fig. 2A), we examined its influence on cancer cell proliferation.

*Acute myeloid leukemia (Kasumi cells).* The first set of experiments was conducted using acute myeloid leukemia because this is the type of cancer cells where upregulation of cholesterol biosynthesis was first reported (21) and because these cells are known to be sensitive to statins (63). VFV and (*S*)-VFV were compared because (*S*)-VFV is a weak inhibitor of human CYP51 (Fig. 2) but has the same structural formula, except for the (*S*) configuration, and thus similar

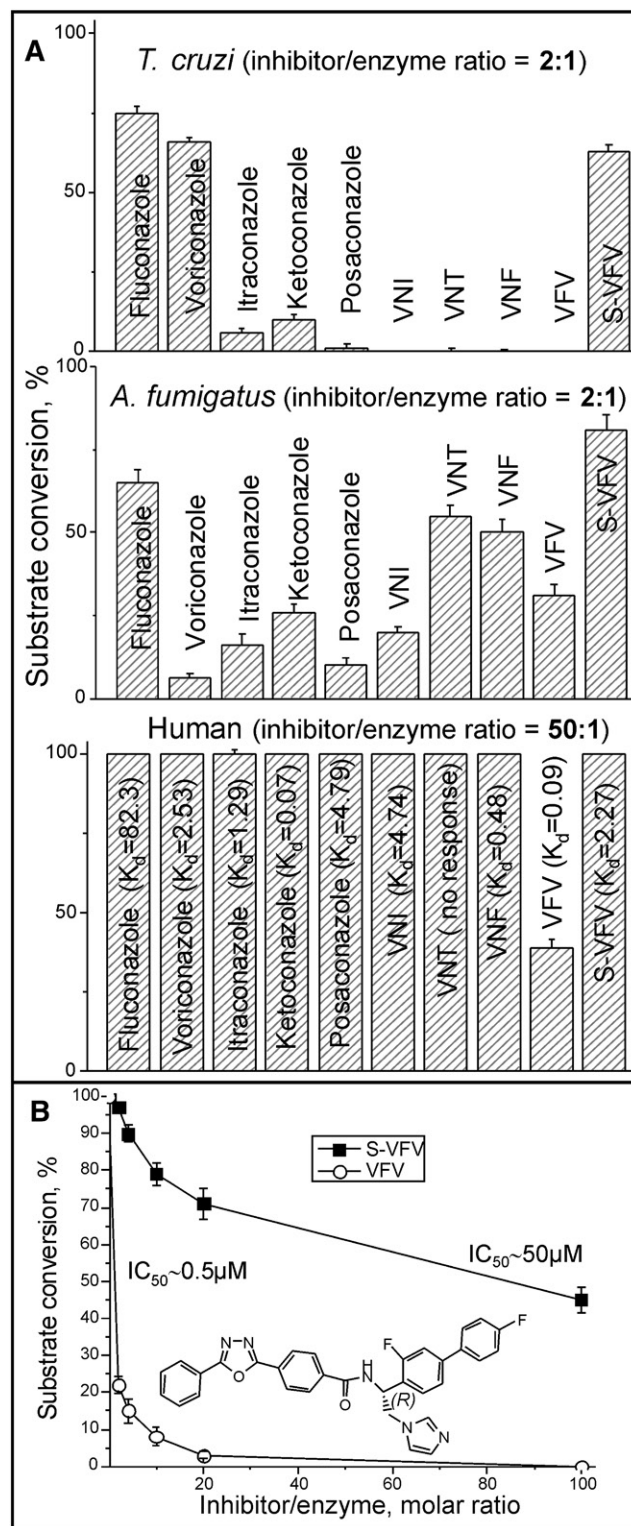


**Fig. 2.** Human CYP51 is resistant to inhibition. A: Inhibitory effects of systemic clinical antifungal drugs and experimental inhibitors on the activity of protozoan (*T. cruzi*), fungal (*A. fumigatus*), and human CYP51 orthologs; 60 min reaction. The spectral  $K_d$  values ( $\mu$ M) for human CYP51/inhibitor complexes are provided in parentheses; see also Fig. 5. B: Inhibitory effects of (*S*)-VFV on the initial rates of the human CYP51 reaction. The chiral C-atom of VFV is marked. The results are presented as mean  $\pm$  SEM. In all experiments the P450 concentration was 0.5  $\mu$ M.

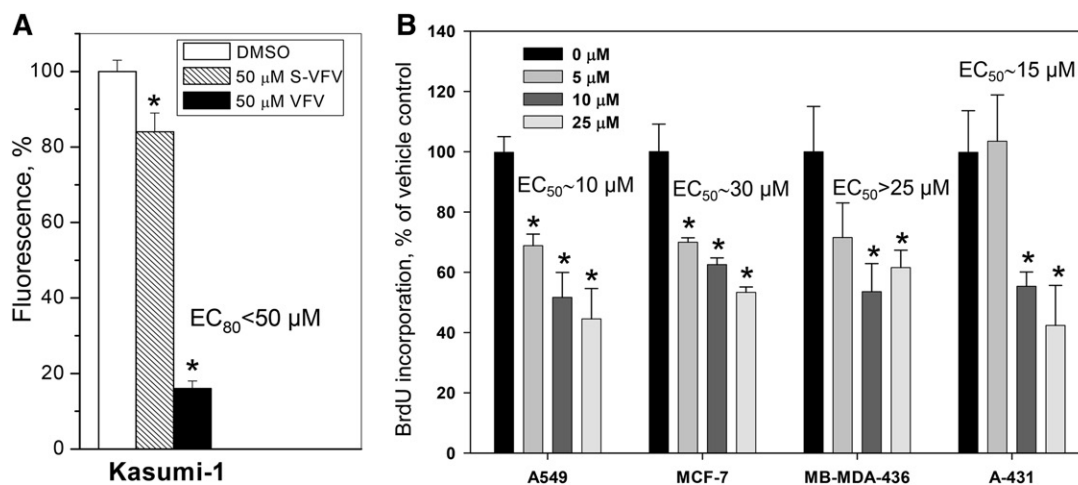


**Fig. 3.** VFV inhibits proliferation of different types of cancer cells. A: Kasumi-1 cells were treated with 50  $\mu$ M VFV or (*S*)-VFV (from a 5 mM stock solution in DMSO) or the vehicle (1% DMSO, v/v) for 7 days. Cell proliferation was evaluated by Alamar Blue fluorescence as described in Materials and Methods. B: Lung (A549, alveolar adenocarcinoma), breast (MCF-7 and MB-MDA-436, hormone-responsive and hormone-nonresponsive adenocarcinomas, respectively), and skin (A-431, epidermoid carcinoma) cancer cells were plated in 96-well tissue culture plates and treated 6 h later with VFV (5–25  $\mu$ M, from 100-fold stock solutions in 25% DMSO and 34% HPCD, v/v) or the vehicle for 24 h. Cell proliferation was evaluated by measuring BrdU incorporation as described in Materials and Methods. The bar graphs show mean cell proliferation presented as percent of vehicle control and SEM of three independent experiments. \* $P \leq 0.05$  compared with 0  $\mu$ M.

cellular permeability, pharmacokinetics, and other drug-like properties (48). The (*S*)-VFV (50  $\mu$ M) decreased proliferation of Kasumi cells by 16% relative to the control (DMSO-treated cells), while the inhibitory effect of VFV was 84% (Fig. 3A).

*Lung cancer, hormone-responsive and -nonresponsive breast cancer, and skin cancer cells.* Four more different types of cancer cell lines were used with 5–25  $\mu$ M VFV (added from 100 $\times$  stocks in 25% DMSO/34% aqueous HPCD) (Fig. 3B). These changes were introduced to test whether the effects could be observed at lower VFV concentrations because the presence of HPCD substantially reduces spectrally detectable (62) precipitation of the compound in

aqueous solutions. The proliferation rates of each of the four types of cancer cells were decreased by VFV in a concentration-dependent manner, with the weakest inhibitory effect being observed in the invasive breast ductal carcinoma line (MB-MDA-436, hormone-nonresponsive breast cancer) ( $EC_{50} > 25 \mu$ M) and the strongest ( $EC_{50} \sim 10 \mu$ M) in the alveolar adenocarcinoma cells (A549, lung cancer) and epidermoid carcinoma cells (A431, the skin cancer) ( $EC_{50} \sim 15 \mu$ M).

The  $EC_{50}$  values of VFV in human cancer lines were substantially higher than those produced in the multiplying stages of protozoan pathogens [ $EC_{50} \sim 1$  nM in amastigotes of Tulahuén *T. cruzi* and 420 nM in intramacrophage amastigotes of *Leishmania infantum* (62)], but they correlate

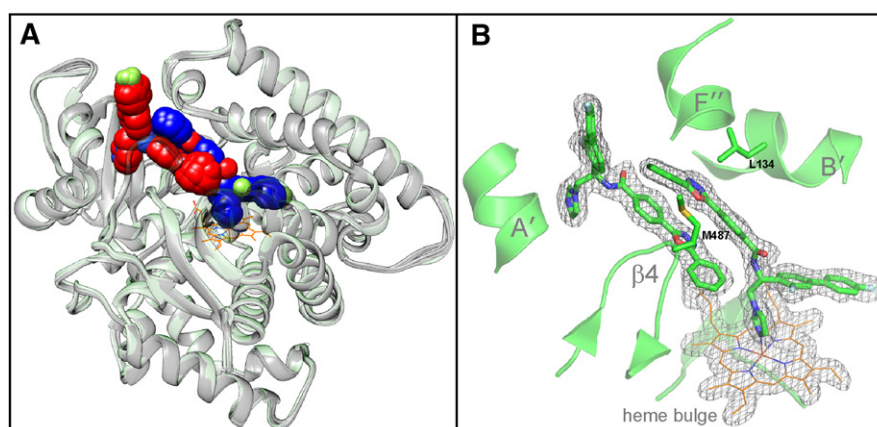


**Fig. 4.** Crystal structures of human CYP51 in complex with VFV. A: Superimposition of four monomers from 4UHI and eight monomers from 4UHL; rms deviation for the C $\alpha$  atom positions  $0.34 \pm 0.06$  Å. One heme molecule (orange lines) is outlined for clarity. All VFV molecules are shown as sphere representation. The C-atoms in the heme-coordinating VFV molecules are blue and in the substrate entry shielding VFV molecules are red. B: The 2Fo-Fc omit electron density map around the CYP51 heme and two VFV molecules, contoured at 1.5  $\sigma$ . Orientation is as in part (A). Some secondary structural elements and the pair of substrate channel gating residues (Met484 and Leu134) are also shown.

with the differences in the potencies of VFV to inhibit protozoan versus human CYP51 enzymes (Fig. 2A). The effects are stronger after longer cell growth periods (Fig. 3A vs. Fig. 3B) [as reported for statins (63)] because several cell cycles are necessary to exhaust the endogenous reserve of cholesterol. The effectiveness of VFV against cancer cells is already within the range of cellular potencies of statins [e.g., (33, 47, 63)] and approaching a mean concentration reported for clinical anticancer drugs (1–10  $\mu\text{M}$ ) (64). Thus, these results serve as an initial proof of concept, encouraging searches for stronger human CYP51 inhibitors.

### Structural characterization of human CYP51 in complex with VFV

To better understand the structural aspects that govern CYP51 catalysis and susceptibility/resistance to inhibition and to explore the molecular basis for the stronger potency of VFV, we determined the X-ray structures of human CYP51-VFV complexes. The complex cocrystallized in the monoclinic  $C_{121}$  space group (2.0  $\text{\AA}$  resolution) contained four monomers in the asymmetric unit. The complex cocrystallized in the triclinic P1 space group (2.5  $\text{\AA}$  resolution) formed an asymmetric unit that included eight monomers (Table 1).

In both cases, regardless of the space group and crystallization conditions, each of the CYP51 molecules had two molecules of VFV bound within the active site (Fig. 4A). One of the ligand molecules (VFV1) is coordinated to the P450 heme iron, while the second (VFV2), rotated  $\sim 180^\circ$  relatively to the first one, “shields” the entrance into the substrate channel. The electron density for both VFV molecules is very well defined (e.g., 2Fo-Fc map; Fig. 4B). This appears to be the first example of 2:1 ligand/CYP51 stoichiometry.

Although binding of VFV2 is not reflected in the “type II” spectral response of human CYP51 (Fig. 5), probably suggesting the lack of cooperativity in the interaction, we believe that its presence in the structure is very unlikely to be a crystallization artifact because: *i*) we observed very good spatial superimposition of the inhibitors (in particular, the noncoordinated molecule) in all 12 complexes, regardless of the space group (Fig. 4A); *ii*) the molar ratio of VFV/P450 in the crystallization samples that produced the  $C_{121}$  space group was only 2.5:1; and *iii*) the complex crystallized in the P1 space group was obtained after human CYP51 copurification with 10  $\mu\text{M}$  VFV, excess ligand being removed during concentration.

The second VFV molecule may play a role in blocking the entrance into the substrate access channel and, thus, somehow “take over” the function of the pair of channel gating residues [i.e., consider “weak” Leu134 and Met487 in human CYP51 (Fig. 4B) vs. “strong” Phe105 and Met460 in *T. brucei* CYP51]. This pair of residues, as predicted by random acceleration molecular dynamic simulations (65), must be important in guiding the passage of CYP51 ligands through the substrate channel, contributing to the human CYP51 fast catalytic rate, broader substrate binding profile, and easier egress of ligands from the active site. Thus, VFV2 may be helpful in the retention of VFV1 within the human CYP51 substrate binding cavity.

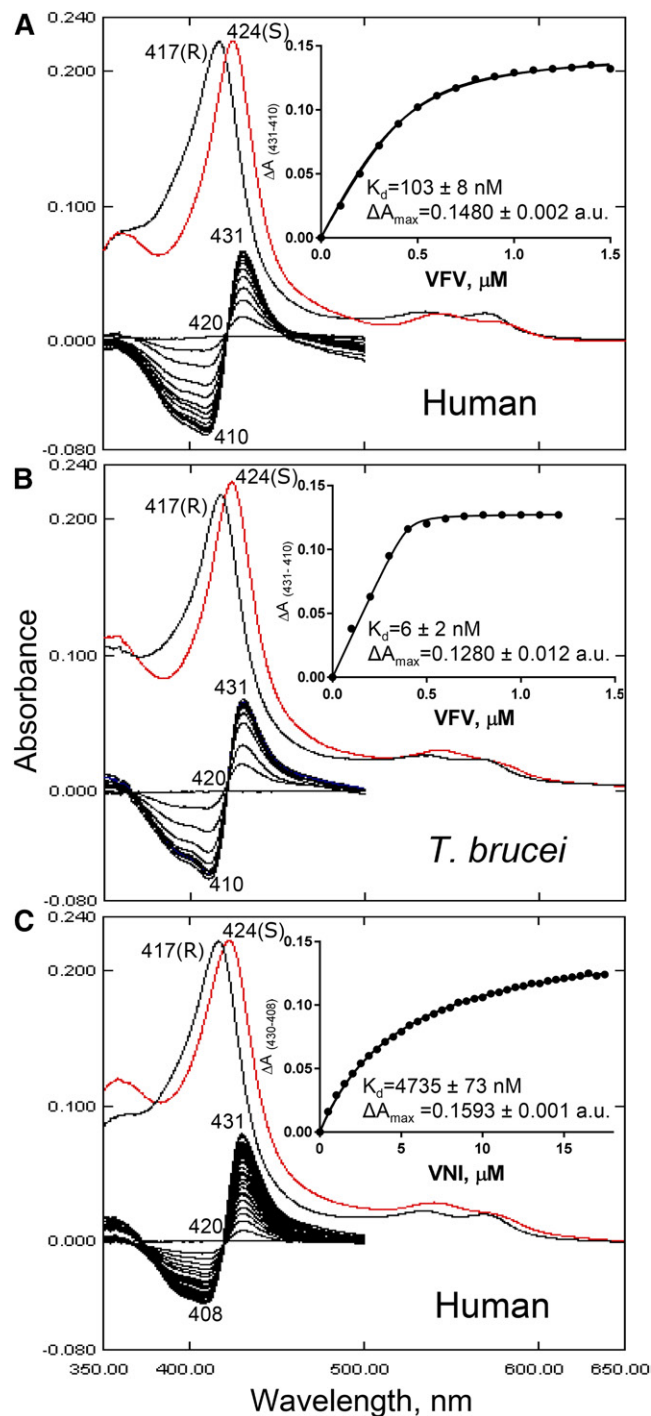


**Fig. 5.** CYP51 spectral response to the addition of heme-coordinating inhibitors. A: Human CYP51-VFV. Absolute (top) and difference (bottom) absorbance spectra. The wavelengths of the Soret band maxima for the peak, isosbestic point, and trough in the difference absorbance are marked, along with the peaks in the absolute spectra. S, sample (after saturation with the inhibitor, red curve); R, reference (difference spectra made by subtracting R from S). Each titration curve is presented in the inset. The shapes of the curves are not sigmoidal, indicating that binding of the second VFV molecule is not reflected in the P450 spectral response. Spectral responses of *T. brucei* CYP51 to VFV [1:1 stoichiometry of the complex (PDB ID 4G7G)] (B) and human CYP51 to VNI (C) are presented for the comparison. The corresponding calculated  $K_d$  values are given (see also Fig. 2). The P450 concentration was  $\sim 0.4 \mu\text{M}$ , and the optical path length was 5 cm.



When the VFV-bound human CYP51 structure is superimposed with the structure of its complex with ketoconazole (3LD6, 2.8 Å) (66), only minor conformational rearrangements in the protein are observed, the root-mean-square (rms) deviation for the C $\alpha$  atom positions being 0.6 Å (Lsqkab). The substrate channel entry is open slightly wider, apparently to accommodate VFV2 (**Fig. 6A**). The FG loop region undergoes the largest movement, with backbone atoms shifting  $\sim$ 2.5 Å. The backbone of the A'-helix repositions by  $\sim$ 1.0 Å, and the movements at the tip of the  $\beta$ 4-hairpin are within 1–1.5 Å. Inside the substrate binding cavity, VFV1 is positioned further away from the heme plane than the molecule of ketoconazole in 3LD6 (**Fig. 6B**). As a result, VFV1 approaches helices B', F'', and I, forming van der Waals contacts (distance  $<$ 4.5 Å) with 21 amino acid residues: Val130, Tyr131, Leu134, Thr135, and Phe139 ( $\alpha$ B'), Ala144 and Tyr145 ( $\alpha$ B''), Phe152 and Leu159 ( $\alpha$ C), Phe234, Ser235, His236, and Trp239 ( $\alpha$ F''), Met304, Gly307, Leu308, Leu310, Ala311, and Thr315 ( $\alpha$ I), Ile377 ( $\beta$ 1-4), and Met487 ( $\beta$ 4-hairpin). [For comparison, ketoconazole contacts 16 human CYP51 residues (not shown).] This is the second largest number of ligand-contacting residues reported to date for the CYP51-inhibitor complexes, the largest set (24 residues) being involved in the interaction of *T. cruzi* CYP51 with posaconazole (60). However, the inhibitory effect of posaconazole on *T. cruzi* CYP51 (see **Fig. 2A**) is at least two orders of magnitude stronger than the effect of VFV on human CYP51 and the

difference in potency is unlikely to be the result of only two additional van der Waals contacts, implying that there are specific structural features (or their combination) that distinguish human CYP51 from fungal and protozoan orthologs, making it resistant to antimicrobial agents.

Comparative analysis of protozoan and human CYP51 structures leads to the hypothesis that the reduced susceptibility to inhibition is connected with the middle portion of the human CYP51 I-helix (8, 60) (the core helix in the P450-fold). First, in human CYP51, this portion of helix I lies 1.5–2.0 Å further away from the heme than it does in the protozoan (**Fig. 6C**) or fungal (50) structures. Protozoan and fungal I-helices are likely to hold the inhibitor more tightly, acting as a “seat-belt” that supports coordination of the inhibitor to the heme iron. Second, in this region of helix I, there is a phylum-specific residue (9, 50) whose side chain is exposed in the CYP51 active site. This is always a bulky phenylalanine in protozoa, plants, and bacteria, leucine in animals (Phe290 and Leu310, respectively, in **Fig. 6C**), and methionine in fungi. The small leucine residue here may contribute to the resistance of human (mammalian) CYP51 to inhibition by further increasing the volume of the enzyme binding cavity. Third (and we believe, most important), the human CYP51 I-helix has a six-residue long (Gly312-Ser316) low energy loop-like segment (**Fig. 7A**), where the main-chain helical hydrogen bonds are missing. Disruption of the hydrogen bond network should make this area of the protein more dynamic. The higher flexibility may, in turn, play a role

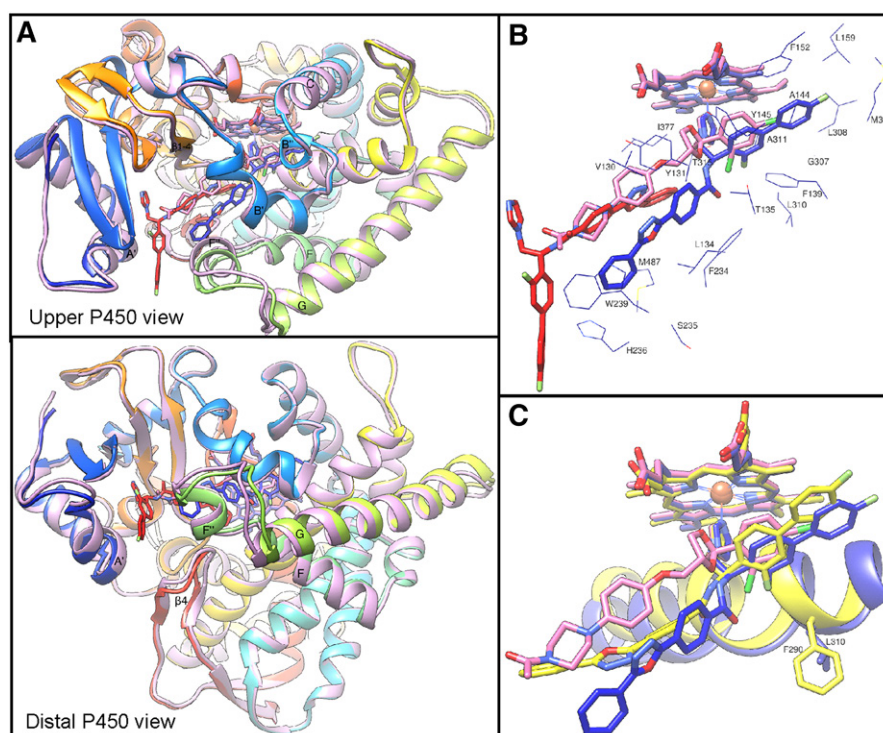


**Fig. 6.** Superimposition of human CYP51-VFV, human CYP51-ketoconazole (pink), and *T. brucei* CYP51-VFV (yellow) complexes. A: Differences in the substrate entry area. The protein ribbon in the complex with VFV is rainbow colored. Some secondary structural elements are marked as references. B: VFV and ketoconazole in the structures of human CYP51. The color of the heme corresponds to the color of the ligand. Side chains of the VFV1-contacting residues are shown. C: The I-helix in the human (blue) versus VFV-bound *T. brucei* (yellow) CYP51 structures.

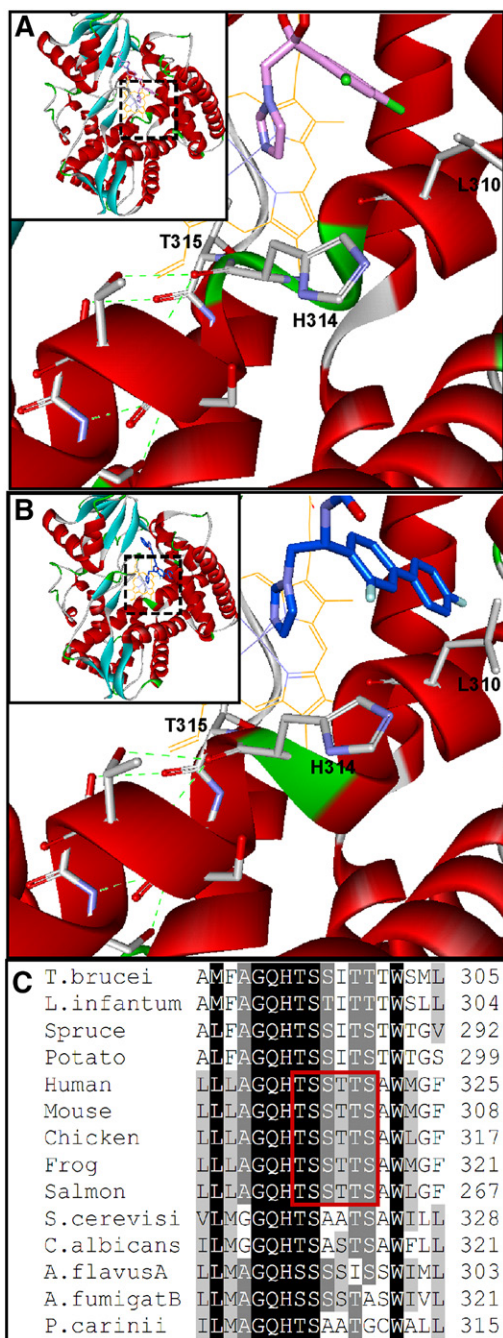


**Fig. 7.** The middle portion of helix I in human CYP51 (Accelrys). A: Complex with ketoconazole. B: Complex with VFV. Inset: Overall view, enlarged areas are framed. The protein ribbon is colored by secondary structure. The loop-like segment in the middle portion of the I-helix is green. Leu310, His31, and the following six polar residues [whose side chains serve as the H-bond (green dashes) acceptors] are shown. C: CYP51 family multiple sequence alignment in the middle of the I-helix. The polar -TSSSTTS- sequence conserved in animal CYP51 enzymes is framed.

in relaying conformational information between different structural elements or even different functional regions of the CYP51 molecule (e.g., acting in combination with the substrate channel gating residues, it might modulate opening/closing of the substrate access channel). Because no loop-like segments are seen in the I-helices of the protozoan

[supporting Fig. S8 in (60)] or fungal [Fig. 16 in (50)] CYP51 structures, the reason for this peculiarity of human CYP51 must be sequence-related. Multiple sequence alignment (Fig. 7C) suggests that it could be the -T<sub>315</sub>SSTTS- sequence that follows the invariant CYP51 family signature histidine, the residue involved in proton delivery (9) (His314 in human CYP51, Thr315 being the conserved P450 threonine). Such a long sequence of polar side chains that serve as the H-bond acceptors is unique (and conserved) throughout animal CYP51 sequences. In the CYP51 orthologs from all other biological kingdoms, there are always one or more nonpolar residues that interrupt this threonine/serine succession.

Interestingly, binding of VFV partially restores the helical structure, shortening the loop-like segment (Fig. 7B). Although the carboxamide nitrogen of VFV does not form any H-bonds with the protein [as it does in the VFV (62) and VNI (51) complexes with the protozoan CYP51], the *ortho*-F atom at the  $\beta$ -biphenyl arm of the inhibitor molecule, being directed right toward the human CYP51 I-helix groove, forms strong (<4.0 Å) van der Waals interactions with Leu310 and Ala311, pushing the latter  $\sim$ 0.6 Å closer to Thr315 (the length of the Ala311 carbonyl-Thr315 carboxyl H-bond is 2.6 Å), and thus apparently strengthening the helix and making this segment of human CYP51 less dynamic. The bulkier substituents in the *ortho*-position of the VFV  $\beta$ -phenyl ring may further stabilize this region of the human enzyme and, thus, further increase the inhibitory potency of our derivatives.

The impact of the I-helix sequence on the human CYP51 resistance to inhibition can be investigated by future site-directed mutagenesis [T318I, L310F, or/and their combination (see Fig. 7C)]. The ultimate goal of our work is to develop human CYP51 cholesterol-lowering agents, focusing on the wild-type enzyme.

#### VFV-Cl as a prototype for structure-based design of more potent inhibitors of human CYP51


We introduced a minimal change into the VFV molecule and synthesized the derivative with a single atom substitution; the fluorine atom in the VFV  $\beta$ -phenyl ring was replaced with the larger chlorine. The structural formula of the compound (VFV-Cl) is shown in Fig. 8, which also compares the inhibitory effects of VFV and VFV-Cl on the activity of human CYP51 at 10-, 25-, and 50-fold molar excess of the inhibitor over the enzyme. Stronger inhibition of human CYP51 by VFV-Cl supports our hypothesis and encourages synthesis of new derivatives with bulkier substituents around the *ortho* C atom of the  $\beta$ -phenyl ring.

#### SUMMARY

To summarize, in comparison with orthologs from other biological kingdoms, human CYP51 has a broader substrate profile, displays faster catalytic rates, and is resistant to inhibition with the azole drugs and drug candidates that target CYP51s of microbial pathogens. VFV, the only

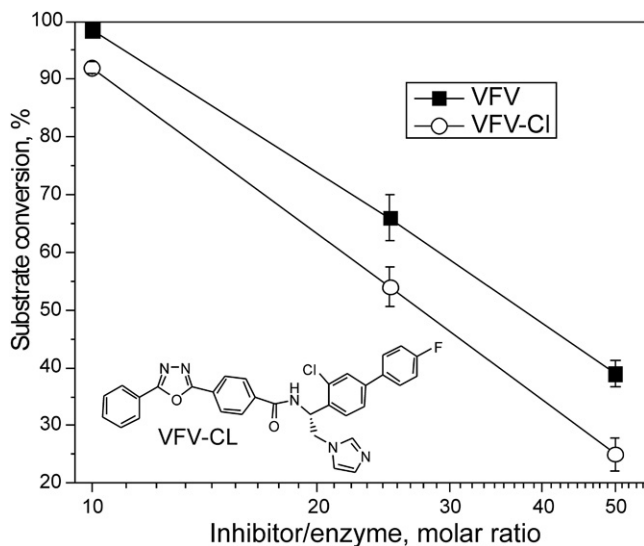


**Fig. 8.** Concentration-response curves of human CYP51 inhibition by VFV and VFV-Cl. The P450 concentration was 0.5  $\mu\text{M}$ , and the lanosterol concentration was 25  $\mu\text{M}$  (60 min reaction). The results are presented as mean  $\pm$  SEM.

fairly potent inhibitor of human CYP51 that we identified, decreases proliferation of various types of cancer cells. Structural characterization of human CYP51-VFV complexes provides an explanation for the weaker susceptibility of human CYP51 to inhibition, offering a visual guide to how the VFV scaffold might be further improved. The stronger inhibitory potency of VFV-Cl suggests work on structure-based design of new compounds to inhibit human CYP51 with potency comparable to antimicrobial drugs that inhibit CYP51 enzymes of human pathogens. Our results indicate that although human CYP51 is not inhibited by known antimicrobial agents, it is drugable and has potential as a target for anticancer therapy. As in any kind of drug development, it is difficult to predict in vivo doses from in vitro potency data. The micromolar values of VFV for human CYP51 inhibition and for anti-proliferative effects on cancer cells may not be low enough to qualify this compound as a clinical candidate, but VFV can serve as a proof-of-concept for the development of more potent inhibitors. As potential anticancer agents, human CYP51 inhibitors are expected to have generally the same mode of action as statins in vivo, yet present certain important advantages. First, their specificity for the biosynthesis of cholesterol would help to avoid side effects of statins due to inhibition of other metabolic pathways. Second, as with systemic clinical antifungal azoles, which kill pathogenic cells that invade multiple organs and tissues, they should have broad tissue distribution. Finally, because all mammalian CYP51 enzymes share very high amino acid sequence identity (e.g., human/mouse 88%, human/dog 96%), animal in vivo models should produce highly relevant outcomes in preclinical trials. Potent inhibitors of human CYP51 may also have advantages as alternative medications for treatment of other cholesterol-related human diseases. The dual occupancy may be important in the mechanism of human CYP51 inhibition. 

## REFERENCES

- Lepesheva, G. I., and M. R. Waterman. 2007. Sterol 14 $\alpha$ -demethylase cytochrome P450 (CYP51), a P450 in all biological kingdoms. *Biochim. Biophys. Acta.* **1770**: 467–477.
- Bloch, K. E. 1983. Sterol structure and membrane function. *CRC Crit. Rev. Biochem.* **14**: 47–92.
- Nes, W. D. 2011. Biosynthesis of cholesterol and other sterols. *Chem. Rev.* **111**: 6423–6451.
- Nes, W. R. 1974. Role of sterols in membranes. *Lipids.* **9**: 596–612.
- Superko, H. R., K. M. Momary, and Y. Li. 2012. Statins personalized. *Med. Clin. North Am.* **96**: 123–139.
- Vaughan, C. J., and A. M. Gotto. 2004. Update on statins: 2003. *Circulation.* **110**: 886–892.
- Heeres, J., L. Meerpoel, and P. Lewi. 2010. Conazoles. *Molecules.* **15**: 4129–4188.
- Lepesheva, G. I., and M. R. Waterman. 2011. Sterol 14 $\alpha$ -demethylase (CYP51) as a therapeutic target for human trypanosomiasis and leishmaniasis. *Curr. Top. Med. Chem.* **11**: 2060–2071.
- Lepesheva, G. I., and M. R. Waterman. 2011. Structural basis for conservation in the CYP51 family. *Biochim. Biophys. Acta.* **1814**: 88–93.
- Frye, L. L., and D. A. Leonard. 1999. Lanosterol analogs: dual-action inhibitors of cholesterol biosynthesis. *Crit. Rev. Biochem. Mol. Biol.* **34**: 123–140.
- Trzaskos, J. M., S. S. Ko, R. L. Magolda, M. F. Favata, R. T. Fischer, S. H. Stam, P. R. Johnson, and J. L. Gaylor. 1995. Substrate-based inhibitors of lanosterol 14  $\alpha$ -methyl demethylase: I. Assessment of inhibitor structure-activity relationship and cholesterol biosynthesis inhibition properties. *Biochemistry.* **34**: 9670–9676.
- Schroepfer, G. J., E. J. Parish, M. Tsuda, D. L. Raulston, and A. A. Kandutsch. 1979. Inhibition of sterol biosynthesis in animal cells by 14  $\alpha$ -alkyl-substituted 15-oxygenated sterols. *J. Lipid Res.* **20**: 994–998.
- Burton, P. M., D. C. Swinney, R. Heller, B. Dunlap, M. Chiou, E. Malonzo, J. Haller, K. A. M. Walker, A. Salari, S. Murakami, et al. 1995. Azalanstat (RS-21607), a lanosterol 14 $\alpha$ -demethylase inhibitor with cholesterol-lowering activity. *Biochem. Pharmacol.* **50**: 529–544.
- Maulik, M., D. Westaway, J. H. Jhamandas, and S. Kar. 2013. Role of cholesterol in APP metabolism and its significance in Alzheimer's disease pathogenesis. *Mol. Neurobiol.* **47**: 37–63.
- Roy, A., and K. Pahan. 2011. Prospects of statins in Parkinson disease. *Neuroscientist.* **17**: 244–255.
- Malfitano, A. M., G. Marasco, M. C. Proto, C. Laezza, P. Gazzo, and M. Bifulco. 2014. Statins in neurological disorders: an overview and update. *Pharmacol. Res.* **88**: 74–83.
- Chan, K. K. W., A. M. Oza, and L. L. Siu. 2003. The statins as anti-cancer agents. *Clin. Cancer Res.* **9**: 10–19.
- Nielsen, S. F., B. G. Nordestgaard, and S. E. Bojesen. 2012. Statin use and reduced cancer-related mortality. *N. Engl. J. Med.* **367**: 1792–1802.
- Hong, J. Y., E. M. Nam, J. Lee, J. O. Park, S. C. Lee, S. Y. Song, S. H. Choi, J. S. Heo, S. H. Park, H. Y. Lim, et al. 2014. Randomized double-blinded, placebo-controlled phase II trial of simvastatin and gemcitabine in advanced pancreatic cancer patients. *Cancer Chemother. Pharmacol.* **73**: 125–130.
- Bjarnadottir, O., Q. Romero, P.-O. Bendahl, K. Jirstrom, L. Ryden, N. Loman, M. Uhlén, H. Johannesson, C. Rose, D. Grabau, et al. 2013. Targeting HMG-CoA reductase with statins in a window-of-opportunity breast cancer trial. *Breast Cancer Res. Treat.* **138**: 499–508.
- Katz, M. S. 2005. Therapy Insight: potential of statins for cancer chemoprevention and therapy. *Nat. Clin. Pract. Oncol.* **2**: 82–89.
- Boudreau, D. M., O. Yu, and J. Johnson. 2010. Statin use and cancer risk: a comprehensive review. *Expert Opin. Drug Saf.* **9**: 603–621.
- Singh, P. P., and S. Singh. 2013. Statins - the holy grail for cancer? *Ann. Transl. Med.* **1**: 1–3.
- Han, J.-Y., S.-H. Lee, N. J. Yoo, L. S. Hyung, Y. J. Moon, T. Yun, H. T. Kim, and J. S. Lee. 2011. A randomized phase II study of gefitinib plus simvastatin versus gefitinib alone in previously treated patients with advanced non-small cell lung cancer. *Clin. Cancer Res.* **17**: 1553–1560.
- Hede, K. 2011. Hints that statins reduce colon cancer risk finally being put to the test. *J. Natl. Cancer Inst.* **103**: 364–366.
- Freeman, M. R., and K. R. Solomon. 2004. Cholesterol and prostate cancer. *J. Cell. Biochem.* **91**: 54–69.
- Pelton, K., M. R. Freeman, and K. R. Solomon. 2012. Cholesterol and prostate cancer. *Curr. Opin. Pharmacol.* **12**: 751–759.

28. Murai, T. 2012. The role of lipid rafts in cancer cell adhesion and migration. *Int. J. Cell Biol.* **2012**: 763283.
29. Babina, I. S., E. A. McSherry, S. Donatello, A. D. K. Hill, and A. M. Hopkins. 2014. A novel mechanism of regulating breast cancer cell migration via palmitoylation-dependent alterations in the lipid raft affiliation of CD44. *Breast Cancer Res.* **16**: R19.
30. Graziani, S. R., F. A. F. Igrreja, R. Hegg, C. Meneghetti, L. I. Brandizzi, R. Barboza, R. F. Amâncio, J. A. Pinotti, and R. C. Maranhão. 2002. Uptake of a cholesterol-rich emulsion by breast cancer. *Gynecol. Oncol.* **85**: 493–497.
31. Li, Y. C., M. J. Park, S-K. Ye, C-W. Kim, and Y-N. Kim. 2006. Elevated levels of cholesterol-rich lipid rafts in cancer cells are correlated with apoptosis sensitivity induced by cholesterol-depleting agents. *Am. J. Pathol.* **168**: 1107–1118.
32. Hirsch, H. A., D. Iliopoulos, A. Joshi, Y. Zhang, S. A. Jaeger, M. Bulyk, P. N. Tsichlis, S. X. Liu, and K. Struhl. 2010. A transcriptional signature and common gene networks link cancer with lipid metabolism and diverse human diseases. *Cancer Cell.* **17**: 348–361.
33. Pandya, A., P. J. Mullen, M. Kalkat, R. Yu, J. T. Pong, Z. Li, S. Trudel, K. S. Lang, M. D. Minden, A. D. Schimmer, et al. 2014. Immediate utility of two approved agents to target both the metabolic mevalonate pathway and its restorative feedback loop. *Cancer Res.* **74**: 4772–4782.
34. Cham, S., M. Evans, J. Denenberg, and B. Golomb. 2010. Statin-associated muscle-related adverse effects: a case series of 354 patients. *Pharmacotherapy.* **30**: 541–553.
35. Harper, C. R., and T. A. Jacobson. 2007. The broad spectrum of statin myopathy: from myalgia to rhabdomyolysis. *Curr. Opin. Lipidol.* **18**: 401–408.
36. Norata, G. D., G. Tibolla, and A. L. Catapano. 2014. Statins and skeletal muscle toxicity: From clinical trials to everyday practice. *Pharmacol. Res.* **88**: 107–113.
37. Russo, M. W., J. H. Hoofnagle, J. Gu, R. J. Fontana, H. Barnhart, D. E. Kleiner, N. Chalasani, and H. L. Bonkovsky. 2014. Spectrum of statin hepatotoxicity: experience of the drug-induced liver injury network. *Hepatology.* **60**: 679–686.
38. Auer, J., H. Sinzinger, B. Franklin, and R. Berent. 2016. Muscle- and skeletal-related side-effects of statins: tip of the iceberg? *Eur. J. Prev. Cardiol.* **23**: 88–110.
39. Rallidis, L. S., K. Fountoulaki, and M. Anastasiou-Nana. 2012. Managing the underestimated risk of statin-associated myopathy. *Int. J. Cardiol.* **159**: 169–176.
40. Platt, F. M., C. Wassif, A. Colaco, A. Dardis, E. Lloyd-Evans, B. Bembí, and F. D. Porter. 2014. Disorders of cholesterol metabolism and their unanticipated convergent mechanisms of disease. *Annu. Rev. Genomics Hum. Genet.* **15**: 173–194.
41. Tint, G. S., M. Irons, E. R. Elias, A. K. Batta, R. Frieden, T. S. Chen, and G. Salen. 1994. Defective cholesterol biosynthesis associated with the Smith-Lemli-Opitz syndrome. *N. Engl. J. Med.* **330**: 107–113.
42. König, A., R. Happle, D. Bornholdt, H. Engel, and K. H. Grzeschik. 2000. Mutations in the NSDHL gene, encoding a 3beta-hydroxysteroid dehydrogenase, cause CHILD syndrome. *Am. J. Med. Genet.* **90**: 339–346.
43. Krakowiak, P. A., C. A. Wassif, L. Kratz, D. Cozma, M. Kovarova, G. Harris, A. Grinberg, Y. Yang, A. G. Hunter, M. Tsokos, et al. 2003. Lathosterolosis: an inborn error of human and murine cholesterol synthesis due to lathosterol 5-desaturase deficiency. *Hum. Mol. Genet.* **12**: 1631–1641.
44. Murai, T. 2015. Cholesterol lowering: role in cancer prevention and treatment. *Biol. Chem.* **396**: 1–11.
45. Freed-Pastor, W. A., H. Mizuno, X. Zhao, A. Langerød, S-H. Moon, R. Rodriguez-Barrueco, A. Barsotti, A. Chicas, W. Li, A. Polotskaia, et al. 2012. Mutant p53 disrupts mammary acinar morphogenesis via the mevalonate pathway. *Cell.* **148**: 244–258.
46. Platz, E. A., S. K. Clinton, and E. Giovannucci. 2008. Association between plasma cholesterol and prostate cancer in the PSA era. *Int. J. Cancer.* **123**: 1693–1698.
47. Campbell, M. J., L. J. Esserman, Y. Zhou, M. Shoemaker, M. Lobo, E. Borman, F. Baehner, A. S. Kumar, K. Adduci, C. Marx, et al. 2006. Breast cancer growth prevention by statins. *Cancer Res.* **66**: 8707–8714.
48. Hargrove, T. Y., K. Kim, M. de Nazaré Correia Soeiro, C. F. da Silva, D. da Gama Jaen Batista, M. M. Batista, E. M. Yazlovitskaya, M. R. Waterman, G. A. Sulikowski, and G. I. Lepesheva. 2012. CYP51 structures and structure-based development of novel, pathogen-specific inhibitory scaffolds. *Int. J. Parasitol. Drugs Drug Resist.* **2**: 178–186.
49. Lepesheva, G. I., W. D. Nes, W. Zhou, G. C. Hill, and M. R. Waterman. 2004. CYP51 from *Trypanosoma brucei* is obtusifoliol-specific. *Biochemistry.* **43**: 10789–10799.
50. Hargrove, T. Y., Z. Wawrzak, D. C. Lamb, F. P. Guengerich, and G. I. Lepesheva. 2015. Structure-functional characterization of cytochrome P450 sterol 14 $\alpha$ -demethylase (CYP51B) from *Aspergillus fumigatus* and molecular basis for the development of antifungal drugs. *J. Biol. Chem.* **290**: 23916–23934.
51. Lepesheva, G. I., H. W. Park, T. Y. Hargrove, B. Vanhollebeke, Z. Wawrzak, J. M. Harp, M. Sundaramoorthy, W. D. Nes, E. Pays, M. Chaudhuri, et al. 2010. Crystal structures of *Trypanosoma brucei* sterol 14 alpha-demethylase and implications for selective treatment of human infections. *J. Biol. Chem.* **285**: 1773–1780.
52. von Wachenfeldt, C., T. H. Richardson, J. Cosme, and E. F. Johnson. 1997. Microsomal P450 2C3 is expressed as a soluble dimer in *Escherichia coli* following modifications of its N-terminus. *Arch. Biochem. Biophys.* **339**: 107–114.
53. Hargrove, T. Y., Z. Wawrzak, J. Liu, W. D. Nes, M. R. Waterman, and G. I. Lepesheva. 2011. Substrate preferences and catalytic parameters determined by structural characteristics of sterol 14 $\alpha$ -demethylase (CYP51) from *Leishmania infantum*. *J. Biol. Chem.* **286**: 26838–26848.
54. Schenkman, J. B., H. Remmer, and R. W. Estabrook. 1967. Spectral studies of drug interaction with hepatic microsomal cytochrome. *Mol. Pharmacol.* **3**: 113–123.
55. Hargrove, T. Y., Z. Wawrzak, P. W. Alexander, J. H. Chaplin, M. Keenan, S. A. Charman, M. R. Waterman, E. Chatelain, and G. I. Lepesheva. 2013. Complexes of *Trypanosoma cruzi* sterol 14 $\alpha$ -demethylase (CYP51) with two pyridine-based drug candidates for Chagas disease: structural basis for pathogen selectivity. *J. Biol. Chem.* **288**: 31602–31615.
56. Lepesheva, G. I., N. G. Zaitseva, W. D. Nes, W. Zhou, M. Arase, J. Liu, G. C. Hill, and M. R. Waterman. 2006. CYP51 from *Trypanosoma cruzi*: a phyla-specific residue in the B' helix defines substrate preferences of sterol 14alpha-demethylase. *J. Biol. Chem.* **281**: 3577–3585.
57. Lepesheva, G. I., R. D. Ott, T. Y. Hargrove, Y. Y. Kleshchenko, I. Schuster, W. D. Nes, G. C. Hill, F. Villalta, and M. R. Waterman. 2007. Sterol 14 alpha-demethylase as a potential target for antitrypanosomal therapy: enzyme inhibition and parasite cell growth. *Chem. Biol.* **14**: 1283–1293.
58. Friggeri, L., T. Y. Hargrove, G. Rachakonda, A. D. Williams, Z. Wawrzak, R. Di Santo, D. De Vita, M. R. Waterman, S. Tortorella, F. Villalta, et al. 2014. Structural basis for rational design of inhibitors targeting *Trypanosoma cruzi* sterol 14 $\alpha$ -demethylase: two regions of the enzyme molecule potentiate its inhibition. *J. Med. Chem.* **57**: 6704–6717.
59. Potterton, E., P. Briggs, M. Turkenburg, and E. Dodson. 2003. A graphical user interface to the CCP4 program suite. *Acta Crystallogr. D Biol. Crystallogr.* **59**: 1131–1137.
60. Lepesheva, G. I., T. Y. Hargrove, S. Anderson, Y. Kleshchenko, V. Furtak, Z. Wawrzak, F. Villalta, and M. R. Waterman. 2010. Structural insights into inhibition of sterol 14 alpha-demethylase in the human pathogen *Trypanosoma cruzi*. *J. Biol. Chem.* **285**: 25582–25590.
61. Kraus, J. M., C. L. M. J. Verlinde, M. Karimi, G. I. Lepesheva, M. H. Gelb, and F. S. Buckner. 2009. Rational modification of a candidate cancer drug for use against Chagas disease. *J. Med. Chem.* **52**: 1639–1647.
62. Lepesheva, G. I., T. Y. Hargrove, G. Rachakonda, Z. Wawrzak, S. Pomel, S. Cojean, P. N. Nde, W. D. Nes, C. W. Locuson, M. W. Calcutt, et al. 2015. VFV as a new effective CYP51 structure-derived drug candidate for Chagas disease and visceral leishmaniasis. *J. Infect. Dis.* **212**: 1439–1448.
63. Burke, L. P., and C. A. Kukoly. 2008. Statins induce lethal effects in acute myeloblastic lymphoma cells within 72 hours. *Leuk. Lymphoma.* **49**: 322–330.
64. Fallahi-Sichani, M., S. Honarnejad, L. M. Heiser, J. W. Gray, and P. K. Sorger. 2013. Metrics other than potency reveal systematic variation in responses to cancer drugs. *Nat. Chem. Biol.* **9**: 708–714.
65. Yu, X., P. Nandekar, G. Mustafa, V. Cojocar, G. I. Lepesheva, and R. C. Wade. 2016. Ligand tunnels in *T. brucei* and human CYP51: Insights for parasite-specific drug design. *Biochim. Biophys. Acta.* **1860**: 67–78.
66. Strushkevich, N., S. A. Usanov, and H-W. Park. 2010. Structural basis of human CYP51 inhibition by antifungal azoles. *J. Mol. Biol.* **397**: 1067–1078.